Chapter in **Advancing Astrophysics with the SKA – II**

Exploring Activity Across the Stellar Main Sequence with the Sun as a Benchmark

Atul Mohan[1,2] Stephen M. White[3,4] Sven Wedemeyer[5,6] and Vladimir Airapetian[1,7]

[1]*Solar Physics Laboratory, NASA Goddard Space Flight Center, Greenbelt, MD, USA*
[2]*Department of Physics, The Catholic University of America, Washington, DC, USA*
[3]*Space Vehicles Directorate, Air Force Research Laboratory, Kirtland AFB, NM, USA*
[4]*Department of Physics and Astronomy, University of New Mexico, Albuquerque, NM 87106, USA*
[5]*Rosseland Centre for Solar Physics, University of Oslo, Oslo, N-0315, Norway*
[6]*Institute of Theoretical Astrophysics, University of Oslo, Oslo, N-0315, Norway*
[7]*American University, Washington, DC, USA*
E-mail: atul.multiverse73@gmail.com, stephen.white.24@spaceforce.mil, sven.wedemeyer@astro.uio.no, vladimir.airapetian-1@nasa.gov

The active atmospheres of cool main-sequence stars (F-M type) often release a fraction of their stored magnetic energy, producing enhanced emissions (flares) across radio to X-ray wavelengths and associated space weather events like coronal mass ejections (CMEs) and energetic particle events (EPEs). Detailed imaging of active regions and CMEs, and in-situ EPE measurements are possible only in our Sun, making it a benchmark for stellar activity research. Multiwaveband solar imaging datasets let us define robust disk-integrated 'Sun-as-a-star' diagnostics of active region and space weather, extendable to stellar datasets. Radio waveband provide diagnostics of particle acceleration, CMEs and EPEs, essential to model flare events and their space weather impacts. The Square Kilometre Array (SKA) telescopes will facilitate sub-second scale spectropolarimetric imaging of the solar corona across 0.05 - 15 GHz, enabling detailed vertical tomographic studies of the active region across a range of coronal heights. Coupled with high energy instruments, the SKA telescopes will allow well-constrained modeling of large samples of diverse active phenomena and the defintion of robust Sun-as-a-star diagnostics of active region and space weather. Besides, the supreme sensitivity and angular resolution of the SKA telescopes will help detect quiescent and active emissions from several nearby stars. This chapter discusses the importance of comparative solar–stellar studies using Sun-as-a-star diagnostics in understanding activity and associated space weather conditions in stars across the cool main-sequence, and presents some research avenues that will benefit solar and stellar astrophysics.

1 Introduction

Cool main-sequence stars (F–M type; cool stars) host most known habitable-zone exoplanets (Bashi et al., 2020). They possess deep convective envelopes that power strong dynamos that generate strong and dynamic magnetic fields threading across the stellar atmospheric layers (see, Donati and Landstreet, 2009, for a review). The active outer atmospheres in cool stars, including our Sun, are capable of producing major space weather events, including intense hour-long flares across the electromagnetic spectrum, especially in the ultraviolet to gamma ray bands, coronal mass ejections (CMEs), and energetic particle events (EPEs; Kowalski, 2024). The properties of stellar convective envelopes and the emergent properties of magnetic field and activity depend on its rotation period (P_{rot}), effective photospheric temperature (T_{eff}), and age (e.g. Noyes et al., 1984; Stepien, 1994a; Donati and Landstreet, 2009; Vidotto et al., 2014). Cool stars form high ('C') and low ('I') activity populations in the P_{rot} - age -T_{eff} plane (Barnes, 2003; Brown, 2014). The 'C' branch has young (< 1, Gyr), fast-rotating ($P_{rot} \lesssim 5$ days) stars and vise versa for the 'I' branch. Stars migrate from 'C' to 'I' branch as they age, with lower T_{eff} stars migrating earlier. Hence, it is essential to model the atmospheres and emergent activity of stars across P_{rot} - age - T_{eff} plane.

The Sun–Earth system serves as a benchmark for stellar activity and space weather research, providing extensive multiwavelength imaging and in-situ energetic particle datasets from a wide range of space- and ground-based observatories. Data-driven modeling of solar active regions using these datasets can provide unprecedented insight into the drivers of major space weather events and associated active regions. Moreover, because the fundamental physical processes and the standard flare model of magnetic activity generally apply across cool stars (Kowalski, 2024), the decades-long solar activity database provides a template library for developing robust solar disk-averaged (Sun-as-a-star) diagnostics of space weather events and active regions. These diagnostics can be extended to stellar studies that lack spatially resolved observations of active regions and direct measurements of space weather.

The energy-release events triggered by stellar activity are often observed as enhanced emissions or flares across the electromagnetic spectrum from long wavelength radio to γ-ray band. Figure 1a illustrates the standard flare model, in which magnetic reconnection releases a fraction of the stored free energy to accelerate the particles and subsequently heat the atmospheric layers, namely the chromopshere and the corona (e.g. Hirayama, 1974; Shibata et al., 1995; Aschwanden et al., 2014, 2015). Strong flare events can also cause coronal mass ejections (CMEs) and produce major energetic particle events (Gopalswamy, 2003; Yashiro et al., 2006; Gopalswamy et al., 2018; Kazachenko, 2023). The SKA telescopes operate in a frequency range that probes both impulsive and sustained particle acceleration across the corona. They trace the propagation of energetic electrons and CMEs, thereby providing key space weather diagnostics. In particular, type III and type IV radio bursts are produced by accelerated electrons traveling along open field lines and contained in closed magnetic-field structures, respectively, when the electrons accelerated at CME-driven shocks generate type II bursts (McLean and Labrum, 1985). Meanwhile, emissions at other wavelengths provide complementary information on flare evolution. Hard X-ray (HXR) probes the emission from the sudden impact of electron beams in the solar atmosphere. Soft X-rays (SXR) diagnose subsequent coronal heating, while the extreme ultraviolet (EUV) continuum and

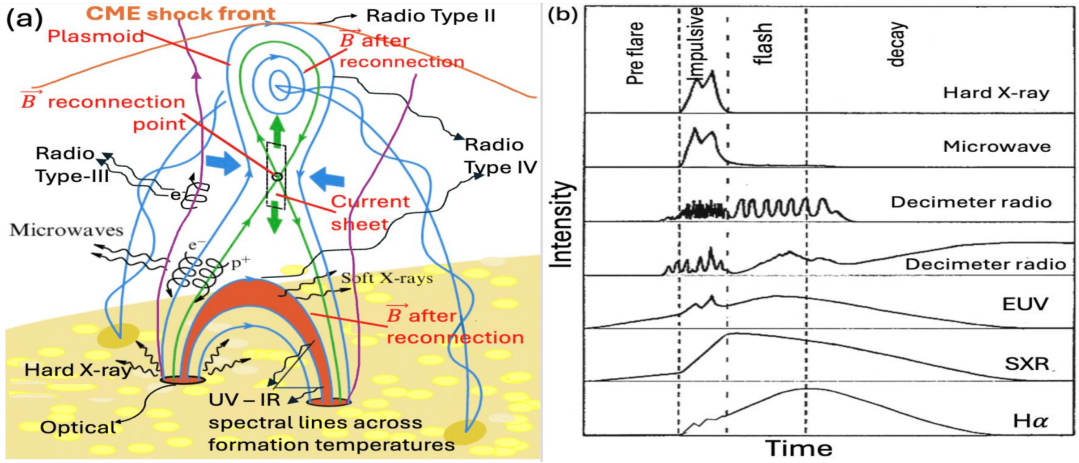

Figure 1: Standard flare model. *(a):* Schematic of the standard model showing the various emission regions. CME shock front (orange), open/closed field lines (violet/blue), and the reconnecting field line (green) are shown (Lysenko et al., 2019). *(b):* Typical Sun-as-a-star multiwaveband light curves from the impulsive non-thermal and the gradual thermal phases, highlighting the Neupert effect (see the text for details).

infrared-to-UV lines probe thermal and non-thermal plasma properties, and bulk flows across the chromosphere and the low corona. Additionally, quasi-steady magnetic activity in active regions, even with weak or often undetectable heating signatures, can produce intense coherent type I radio bursts, offering diagnostics of persistent particle acceleration in the corona (Iwai et al., 2012, 2014; Li et al., 2017; Mohan et al., 2019a). Additionally, solar observations close to 15 GHz can trace the regions of the upper chromosphere associated with coronal holes that power the fast solar wind (Gopalswamy et al., 2000; Akiyama et al., 2013).

Figure 1b shows the typical solar-stellar flare light curves during various flare phases from the preflare to the decay phase. The impulsive phase at the start of the flare is a direct diagnostic of non-thermal particle acceleration and the impact of energetic electron beams in the corona and chromosphere, followed by the gradual heating phase, primarily seen in the high energy continuum emissions. The integral of impulsive phase emission often correlates well with the gradual phase thermal emission, as first noted by Neupert (1968), and henceforth is known as the Neupert effect. The Neupert effect highlights that the energy dissipation by the non-thermal particles produced during the impulsive phase gradually heats the corona.

1.1 Solar-stellar connection

Several stellar flares demonstrate the Neupert effect (e.g. Guedel et al., 1996; Tristan et al., 2023). and show similarities in the timing of the onset and profiles of multiwavelength flares compared to the typical Sun-as-a-star template (Kowalski, 2024). For instance, Fig.4 shows a typical solar radio burst dynamic spectrum (DS) during a fast solar CME with a DS from AD Leo during a major flare (Mohan et al., 2024a,d). Beyond individual flare analogies, universal scaling relations such as the Güdel–Benz law (GBR; Gudel et al., 1993), linking radio and SXR luminosities across solar and stellar flares spanning several orders of magnitude (Benz and Guedel, 1994; Guedel et al., 1995), underscore the shared underlying physics of these phenomena. Additional studies have revealed consistent flux–flux correlations among spectral lines, continua, and surface magnetic flux for the

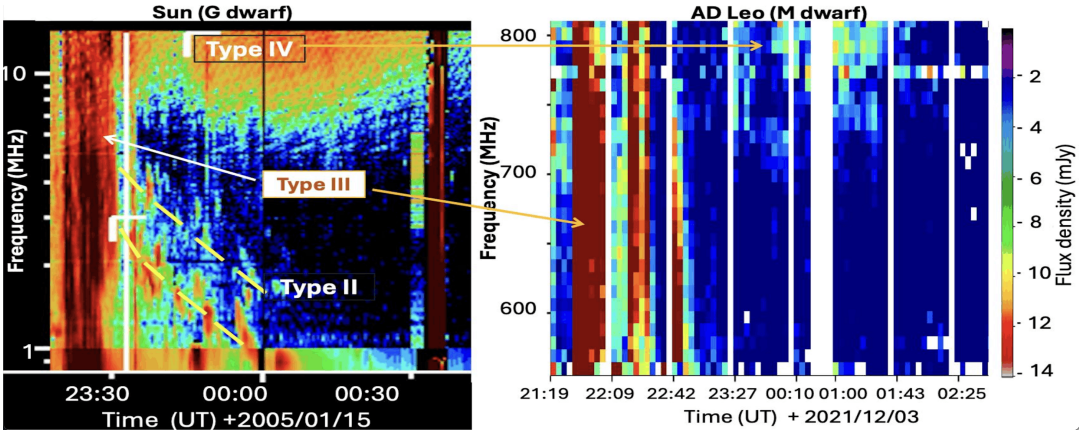

Figure 2: Solar-stellar connection. Comparison of radio DS during a fast solar-CME (STOKES I) and during a burst reported in AD Leo (STOKES V), revealing the various radio burst types Mohan et al. (2024d,b).

Sun and solar-type stars (e.g. Pevtsov et al., 2003; Toriumi et al., 2022). These results highlight the phenomenological correspondence between solar and stellar flares.

Meanwhile, sensitive multiwaveband telescopes capable of observing stellar and solar flares with high sensitivity and spectro-temporal resolution are being commissioned. These sensitive facilities will enable detections of stellar flares over a large sample of stars with varying physical parameters, while also enabling detailed modeling of solar flares and derivation of robust space weather and active region diagnostics. Extending solar-based diagnostics to a statistically significant sample of stellar events will help explore the long-term evolution of activity and associated space weather conditions around Sun-like stars, and contrast solar activity in the context of the broader main-sequence.

1.1.1 Importance of Sun-as-a-star diagnostics in stellar space weather research

Stellar astronomy is in a transformative phase with a new generation of sensitive multiwavelength observatories that are operational or are soon to be commissioned and can detect flares from large stellar samples. However, there are no means yet or in the near future to directly detect and estimate the parameters of flare-associated space weather events or active regions. The vast solar database with detailed multiwaveband flare and associated in-situ EPE data will allow us explore robust Sun-as-a-star flare diagnostics that correlate well with the occurrence and properties of major space weather events and active regions. A set of such robust Sun-as-a-star diagnostics in wavebands that are accessible to stellar research will facilitate the inference of space weather impacts of stellar flares, while also providing a parameter space for comparative solar-stellar activity research.

Several studies have explored Sun-as-a-star diagnostics across multiple wavebands and their correlations with space weather and magnetic field properties. For instance, when it comes to CME diagnostics, flux dimming in EUV and SXR emissions provides a diagnostic of CME mass (Hudson et al., 1996; Harrison et al., 2003; Veronig et al., 2021), while spectral line Doppler shifts and line-width variations yield information on bulk plasma flows (e.g. Namekata et al., 2024). In addition, statistical studies show that the stronger the SXR flare flux, the higher the chances of a CME (Kazachenko, 2023). Nevertheless, the wealth of solar observations shows that many erup-

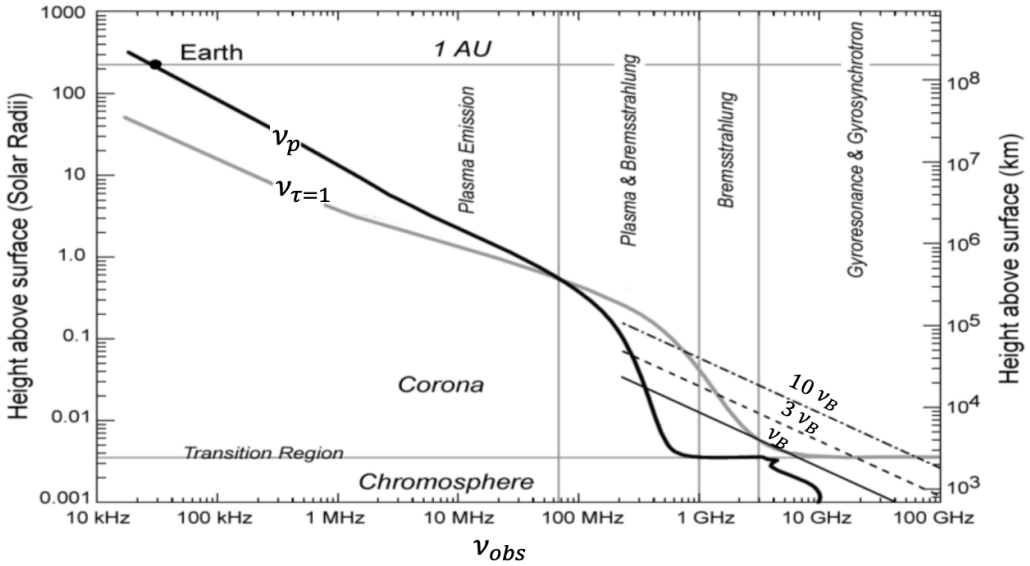

Figure 3: Radio emission mechanisms. The profiles of ν_p and ν_B are shown with the dominant emission mechanisms within various frequency ranges demarcated. The frequency at which optical depth becomes unity is shown as a function of height. The density was computed based on VAL model B (Vernazza et al., 1981) and 5 times the Saito et al. (1970) model. Temperature profile was obtained from the VAL model to about 105 km, and was extended using a hydrostatic equilibrium model. Adapted from Gary and Hurford (2004).

tive (CME-associated) flares lack one or more of these signatures, whereas some strong confined (CME-less) flares exhibit some of them (Nitta and Mulligan, 2017; Veronig et al., 2021). In the case of SXR flares, about 10 - 20% of solar flares belonging to the strongest energy class do not cause CMEs, while several flares belonging to an order of magnitude weaker class are occasionally linked to CMEs. In this context, the relevance of radio diagnostics is notable, with >95% of type II bursts and >81% of type IV bursts associated with CMEs (Kumari et al., 2021b, 2023). The association rates increase to nearly 100% when the radio burst emission is observed to extend from decimetric to decameter-hectometric ranges (Gopalswamy et al., 2005; Gopalswamy, 2011; Miteva et al., 2017; Mohan et al., 2024a).

1.2 Radio diagnostics and their relevance

Solar-stellar radio emission can be produced by five different mechanisms that are well understood and provide complementary diagnostics of physical conditions in the solar atmosphere:

- Bremsstrahlung, also known as free-free emission, is due to the collisions of electrons with ions. At radio wavelengths, the opacity of this mechanism is dominated by thermal electrons and varies as $n^2T^{-1.5}\nu^{-2}$, where n, T, and ν denote the electron density, temperature, and emission frequency. The density dependence makes this a ubiquitous source of radio emission throughout the solar atmosphere.

- Gyroresonance emission results from the opacity of electrons orbiting magnetic field lines at the gyrofrequency (ν_B = 2.8 $|\vec{B}_{Gauss}|$ MHz). Field strengths of order 100 - 1000 G are common in solar active regions, and the corresponding values of ν_B lie in the microwave

range. This mechanism provides high opacity purely due to the presence of ambient thermal plasma and is therefore used to measure coronal magnetic fields (White and Kundu, 1997). This mechanism can produce high degrees of circular polarization depending on whether the sense of polarization matches the sense of rotation of electrons about the magnetic field.

- Gyrosynchrotron emission has the same basic physics as gyroresonance emission, but is produced by nonthermal high energy electrons accelerated in flares. The radio spectrum can provide the physical characteristics of the radiating electrons. A typical flare has a spectral peak due to gyrosynchrotron at around 10 GHz, but in large solar flares, gyrosynchrotron emission can be seen up to hundreds of GHz.

- Plasma emission is responsible for the well-known low-frequency solar radio bursts (Type I-V). It is a coherent mechanism where energetic electron beams efficiently excite electrostatic waves at the Langmuir (or plasma) frequency, $\nu_p = 9000\ \sqrt{n}$ Hz, and get converted to propagating electromagnetic waves at the plasma frequency and its harmonic, $2\nu_p$. Plasma emission is hence a powerful diagnostic of electron beams in the solar atmosphere. However, absorption of plasma emission depends on a high power of electron density, and this limits its occurrence above several hundred MHz on the Sun.

- Electron-cyclotron maser emission (ECM) is another coherent mechanism that produces intense radio bursts in the frequency range around 1 GHz, immediately above the frequency domain dominated by plasma emission. It is produced at $\nu = \nu_B$, and is due to the structure in the 2-dimensional (perpendicular and parallel to the magnetic field) electron velocity distribution that provides free energy for a relativistic resonance. Jovian decametric emission at Jupiter).

Figure 3, adapted from Gary and Hurford (2004), summarizes the dominant emission mechanisms with various spectral bands and the variation of ν_p and ν_B with height based on standard 1D atmospheric models. The plasma emission mechanism powers active solar/stellar emissions in the operational band (0.05–0.35 GHz) of the SKA-Low telescope. The supra-thermal electron beams accelerated at reconnection sites and CME-driven shocks produce various types of radio bursts with characteristic dynamic spectral variability (type I - IV; see Sect. 1), and flux densities exceeding the quiescent emission by several orders of magnitude. These burst types form excellent diagnostics of active regions, CMEs, and solar energetic particle (SEP) events (Gopalswamy et al., 2005; Miteva et al., 2017). Almost all type II bursts and more than 85% of type IV bursts are CME-associated (Gopalswamy, 2000, 2011; Kumari et al., 2023; Hillaris et al., 2016; Mohan et al., 2024a). About 75% of type IV bursts accompany fast, wide CMEs, which are highly geo-effective, often producing strong SEPs (Miteva et al., 2017; Kumari et al., 2021a; Mohan et al., 2024a). Mohan et al. (2024c) further derived relations connecting active-region and CME parameters to Sun-as-a-star type II burst observables and SXR flux. Type III bursts trace electrons propagating along open magnetic field lines, providing direct diagnostics of impulsive SEPs (Cane et al., 2002; Winter and Ledbetter, 2015; Miteva et al., 2017).

Meanwhile, at higher frequencies covered by the SKA-Mid telescope (0.35–15 GHz), both coherent (ECM) and incoherent mechanisms (gyrosynchrotron, gyroresonance) power the emission from

flare-accelerated electrons (see Gary, 2001; Güdel, 2002). The emission mechanisms can be inferred from the dynamic spectral evolution and polarization. Coherent bursts, forming near harmonics of the local ν_p or ν_B enable direct inference of local plasma parameters. Modeling incoherent emission, on the other hand, constrains the electron energy distribution and magnetic field strength in active regions, particularly when combined with spectro polarimetric diagnostics (e.g. Dulk, 1985; Gary et al., 1996; White et al., 2000; Lee et al., 2003; Gary et al., 2018; Alissandrakis and Gary, 2021; To et al., 2023; Kuznetsov et al., 2025).

Several solar studies have also reported quasi-periodic pulsations (QPPs) and fine structures in 0.05 - 15 GHz dynamic spectra, linking them to local plasma or MHD wave processes, density perturbations, and particle acceleration scales in active regions (see, Aschwanden, 1987; Arzner and Magun, 1999; Nakariakov and Melnikov, 2009; Alissandrakis et al., 2023, for a review). The SKA precursors and pathfinders are already making major progress in this field, which will also benefit the exploration of robust Sun-as-a-star metrics and insights extendable to stellar flare studies (e.g. Kontar et al., 2017b; Sharykin et al., 2018; Mohan et al., 2019b; Mohan, 2021b; Mondal and Oberoi, 2021; Mohan, 2021a). Besides their physical relevance, radio bursts frequently outshine the integrated quiescent solar or stellar disk emission by several orders of magnitude, making them excellent Sun-as-a-star activity diagnostics detectable from sources at far greater distances than quiescent stellar emission.

1.2.1 Tomographic exploration with wideband radio imaging spectroscopy

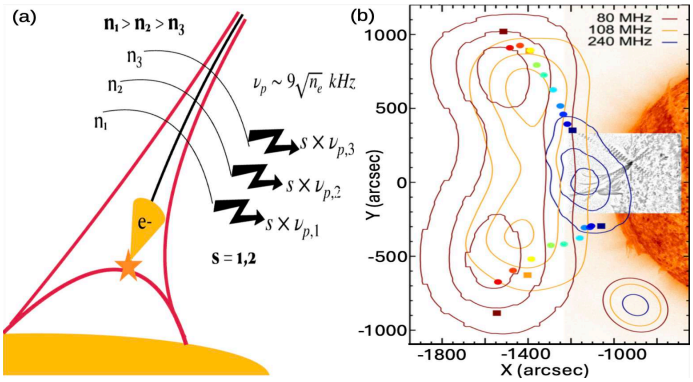

Figure 4: Tomographic exploration using spectroscopic radio imaging. *(a):* Illustration of coherent radio bursts triggered at varying density ((n_i; i$\in$ [1, 3])) regions, located at different heights along the tragectory of an accelerated electron beam. The burst emission occurs at the harmonics (s) of the local ν_p. *(b):* Tomographic mapping of a solar active region using spectroscopic images within 80 - 240 MHz range from the MWA. For each observing frequency, contours at 20, 50, and 80 % of the peak intensity are shown. Colors from red to blue indicate increasing frequency, and marker separation denotes the source size at each frequency. The image contours at various frequencies collectively trace the vertical magnetic structure transporting the flare-accelerated electrons. (McCauley et al., 2017).

The different types of stellar active phenomena energise plasma and accelerate particles across coronal heights, often evolving into major space weather events. Hence, to study the evolution and space weather impacts of an active event, we require a robust tomographic exploration strategy that probes the event-associated dynamics across coronal heights. A strategy to define a tomographic tool is to identify a set of spectral bands sensitive to specific thermal and non-thermal processes within narrow height ranges across the corona to interplanetary space.

Spectral line inversions using simultaneous multi-line data are often used to infer the heights and dynamics of plasma and energetic particles across the chromosphere to the corona. However, various non-local thermodynamic equilibrium (non-LTE) processes and propagation effects introduce degeneracy in the multi-line inversion procedure, making it difficult to accurately infer emission heights (e.g. Mashonkina et al., 2017; Jeffrey et al., 2017; Kontar et al., 2017a; Zhou et al., 2022). Besides, the time resolution obtained in multi-line spectral inversion studies is of the order of ~ 10 s to min even for stellar flares, making it difficult to trace seconds-scale non-equilibrium dynamics, known to exist from high cadence radio and X-ray observations (e.g. Dennis, 1985; Osten et al., 2008; Endo et al., 2010; Saint-Hilaire et al., 2013). Meanwhile, the optically thin coronal plasma continuum in the SXR band provides thermal diagnostics averaged over a very wide height range along the line-of-sight.

In contrast, coherent radio bursts associated with active events form at the harmonics of the local ν_p or ν_B both of which vary with height in the corona (see Fig. 3). This property makes spectroscopic radio imaging across wide bandwidths at sub-second timescales an excellent tool to perform tomographic studies of the onset and propagation of energetic particleas and their progenetors (e.g., CME) across corona and into the interplanetary space causing space weather impacts. Figure. 4a illustrates this idea using a cartoon of an accelerated electron beam propagating along an open magnetic field structure generating coherent bursts at varying frequencies as a function of height. Figure. 4b shows snapshot spectroscopic images from MWA within 80 -240 MHz. The image contours clearly map the vertical structure of the active region magnetic field. Hence, modeling the dynamic spectral variability of the stellar coherent bursts by extending insights and diagnostics from solar studies can help constrain the evolution of energetic particles, instabilities, and their progenetors during active phenomena along the line-of-sight axis, providing valuable insights into the associated space weather impacts.

1.3 Radio instrumentation requirements for comparative solar-stellar studies

The interdisciplinary field of comparative solar-stellar research relies on a Sun-as-a-star analysis framework, which enables robust quantitative comparisons between solar and stellar phenomena. Developing a robust Sun-as-a-star framework requires characterizing the solar emission variability across dimensions of flux density, frequency, time, and polarization in the image plane to identify the sources, understand the drivers of magnetic activity, and define meaningful multi-dimensional diagnostics sensitive to major space weather events and active region properties despite spatial averaging of the data.

The dynamic spectral studies of the Sun and magnetically active stars have reported signatures of polarized emission variability at sub-MHz and sub-second scales. Hence, the identification and tracking of flaring regions require wideband spectro-polarimetric imaging at sub-MHz and sub-second scales with sub-arcmin angular resolution, necessary to resolve active regions. Additionally, there can be multiple co-temporal active events on the solar disk capable of producing radio bursts that are brighter than the event of interest by several orders of magnitude. So, robust tracking of the evolution of a single event in the image plane requires high fidelity and high dynamic range imaging capability, which directly translates to the need for dense instantaneous *uv*-plane coverage enabled by a compact core large-N array configuration.

On the stellar side, we require the capability to perform polarimetric imaging of stellar fields with high spectro-temporal resolution comparable to solar observations. To study activity across the cool main sequence, wideband, long-term monitoring datasets are required for stars spanning a range of P_{rot}, age, and T_{eff} values. For meaningful comparisons with the Sun, target stars should be either isolated or members of non-interacting binary systems with a typical separation of $\gtrsim$20 AU like the α Cen AB. Telescopes with high sensitivity and angular resolution of the order of a few arcseconds to sub-arcseconds are therefore essential for generating large samples of such stars by scanning sources within several tens to a few hundred parsecs.

To quantitatively assess the sensitivity requirements, let us consider the Sun and AD Leo, an active star located at 5 pc. The typical solar quasi-steady flux can vary during its activity cycle within 50 - 100 SFU (White, 2004; Shibasaki et al., 2011; Shimojo et al., 2017) in the 0.05 - 0.35 GHz range (SKA-Low's operational band), while in 0.35 - 15.4 GHz range (SKA-Mid's operational band), the flux can be about a few to 60 SFU (McLean and Labrum, 1985; Oberoi et al., 2017). If Sun were located at 1 pc, its disk-integrated quiescent flux would be ~0.5 -30 μJy in the SKA-Low's and ~ 25 - 50μJy in the SKA-Mid's operational bands. Additionally, solar radio bursts can be 1 - 2 or 3 - 6 orders of magnitude brighter than the quiescent emission (see, Saint-Hilaire et al., 2013; Nindos et al., 2000; Reid and Ratcliffe, 2014). Likewise, if AD Leo were located at 1 pc, it would have a quasi-steady flux of ~50-100 mJy in the 0.5 - 1 GHz range (Villadsen and Hallinan, 2019; Mohan et al., 2024d). During strong flares, AD Leo can be 10 – 1000 times brighter than the quiescent level (White et al., 1989; Osten and Bastian, 2006; Villadsen and Hallinan, 2019).

2 Advancements with the SKA telescopes

The SKA telescopes will facilitate sensitive sub-second sub-MHz snapshot spectro-polarimetric solar and stellar imaging observations in the 0.05 - 15 GHz range. The large-N architecture of the SKA telescopes will enable high-fidelity imaging required for solar activity studies. The telescopes will offer significantly higher sensitivity across their operational bands than current state-of-the-art facilities, owing to their higher collecting area (A_e) and lower system temperature (T_{sys}) values. Besides, owing to their long baselines, the angular resolution of the SKA telescopes will be an order of magnitude finer than the leading telescopes in the 0.05-15 GHz range.

2.1 SKA-Mid in AA4 and AA* configurations

The SKA-Mid telescope, planned to operate over 0.35 - 15.4 GHz, will enable high dynamic range imaging at about 0.14 s and 13 kHz resolution, with an angular resolution of about $0.23'' \times 0.2''$ in the AA4 configuration at 1.4 GHz. Meanwhile, the resolution for the AA* configuration is expected to be about $0.78'' \times 0.29''$. This is a significant improvement compared to the few arcsec resolution offered by the solar imaging mode of the Jansky Very Large Array (JVLA)[1] and the $0.25''$ resolution offered by the most extended JVLA configuration for general astronomical observations. The sensitivity (measured as A_e/T_{sys}) of the AA* (AA4) array at 1.4 GHz is expected to be about 6(8) times better than MeerKAT (Jonas and MeerKAT Team, 2016), which is an SKA precursor. The AA*(AA4) array would help achieve a root mean square (RMS) noise level of 15.8(10.2) μJy/beam

[1] https://science.nrao.edu/facilities/vla/docs/manuals/obsguide/modes/solar

with 1 h and 0.81 GHz averaging in Band 2, centered at 1.4 GHz. This sensitivity will let us detect quiescent emission from stars like AD Leo out to 25 (30) pc using the AA*(AA4) array configuration, with 5σ detection significance. On the contrary, significant detections of radio bursts from stars at similar distances will be possible with temporal averaging of 0.1–1 s and spectral averaging of 0.1–1 MHz. The strongest class of coherent bursts could be detected with similar spectro-temporal averaging by AA* and AA4, from stars at distances of ∼0.1 kpc. At 0.1 kpc, 20 AU corresponds to 0.2″, which will be barely resolved by the AA4 configuration, while AA* will resolve all binaries with a separation >80 AU and located at distances up to 0.1 kpc.

2.2 SKA-Low in AA4 and AA* configurations

The sensitivity of the SKA-Low telescope (operational band: 0.05 - 0.35 GHz) at 70 (200) MHz will be ∼120 (400) m^2/K in AA* and 200 (600) m^2/K in AA4 configurations. At 70 (200) MHz, the AA* array will be ∼ 15 (5) and AA4 about 28 (7.5) times better in sensitivity than the SKA pathfinder, LOw Frequency ARray (LOFAR; van Haarlem et al., 2013). In the 0.2-0.5 MHz range, the sensitivity of the SKA-Low telescope will be higher than the state-of-the-art instrument, the upgraded Giant Meterwave Radio Telescope (uGMRT Gupta et al., 2017), by a few factors. The SKA-Low telescope will achieve an RMS noise level of 81 (132) μJy with 1 h integration at 200 MHz in AA4 (AA*) configuration, with an angular resolution of ∼3.89″.

The high sensitivity and large fields of view of the SKA telescopes directly translate to orders of magnitude higher survey speeds in the radio band, compared to the current state-of-the art facilities. The faster survey speeds coupled with high sensitivity will help generate large samples of stellar flares with significantly less telescope time. Additionally, the imaging high dynamic range will advance solar activity and Sun-as-a-star research. All sensitivity estimates presented here are based on the Square Kilometre Array Observatory's sensitivity calculator[2] and the data released by the observatory online[3].

3 Research avenues

A combined solar-stellar flare and space weather analysis framework is essential to infer not only the space weather relevance of flares across the stellar main-sequence but also to compare solar atmospheric structure and activity against other main-sequence stars across the P_{rot}-T_{eff}-age. Comparative solar stellar studies focusing on Sun-like G dwarfs of varying ages can also provide a picture of solar activity evolution across ages and test the applicability of the standard flare model and emission mechanisms across a wide range of flares in stars with different atmospheric plasma and magnetic field parameters. The following subsections will discuss some of the solar-stellar research avenues that will benefit from the SKA telescopes.

3.1 Sun-as-a-star classification scheme for solar-stellar activity

As discussed in Sect. 1.2, there are multiple emission processes in the broader radio wavelength range, and the dominance of the emission process depends closely on the local plasma and

[2] https://sensitivity-calculator.skao.int/

[3] https://www.skao.int/en/science-users/118/ska-telescope-specifications

magnetic field parameters and their variability scales (Gary, 2001; Zhang et al., 2024). Hence, depending on atmospheric physical parameters, different emission mechanisms may dominate within a given observing frequency range for different stars. There have been reports of mixed emission mechanisms and deviations from the general picture presented in Fig. 3 even for solar radio bursts (e.g. Morosan et al., 2016; Carley et al., 2019; Morosan et al., 2019). In addition,

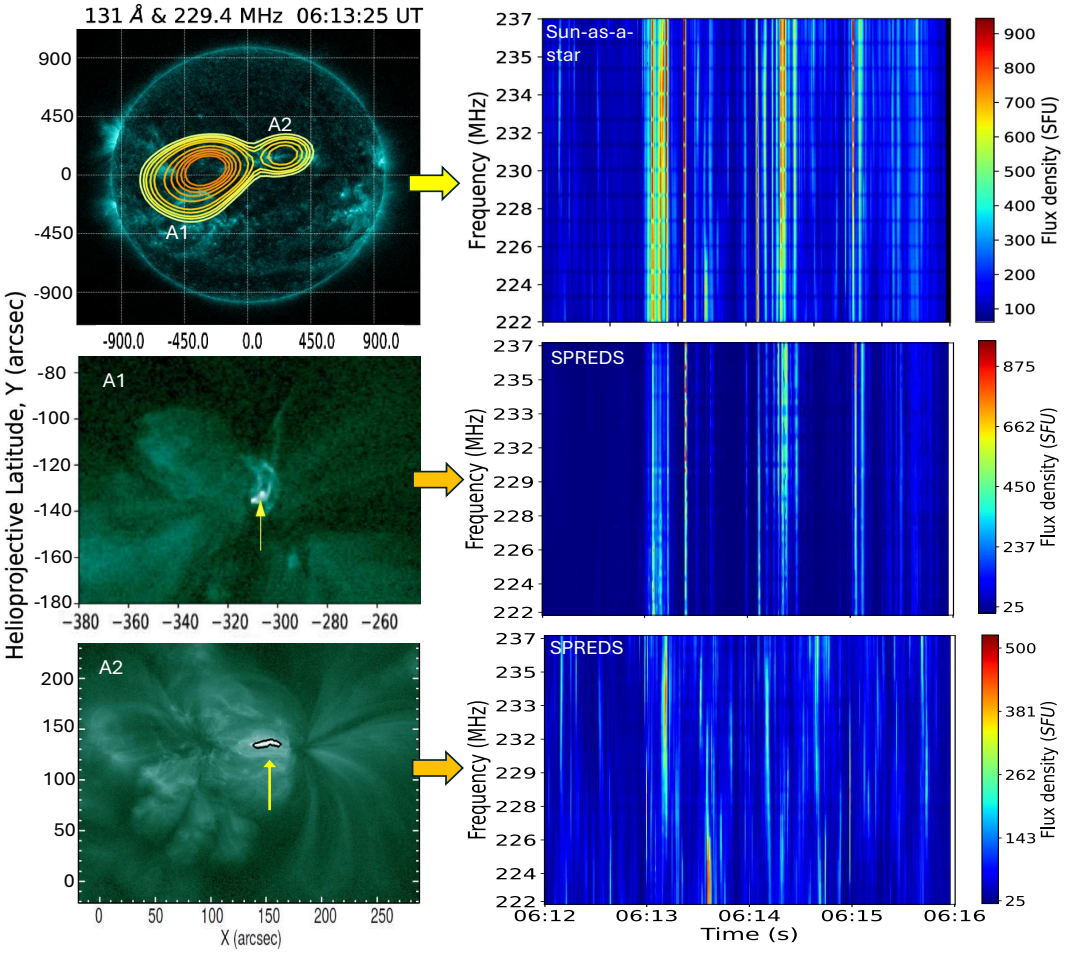

Figure 5: *Top:* A sample radio contour map of the Sun from Nov 3, 2014, overlaid on co-temporal EUV image at 94Å from SDO/AIA instrument. Radio contours are marked at 0.5, 0.7, 0.9, 1.3, 1.8, 3.6, 5.4, 7.2, 9, and 11 $\times 10^8$ K to highlight the co-temporal radio burst sources, A1 and A2. A Sun-as-a-star/total flux density dynamic spectrum is shown on the right. *Middle:* A1 region overlaps an active region that produced a weak coronal jet (arrow). SPREDS for A1 reveals quasi-periodic type III bursts. *Bottom:* A2 overlaps an active region that produced a confined microflare (arrow). SPREDS for A2 reveals numerous coherent emission fine structures ($\delta t \lesssim 2\,s$; $\delta\nu \sim$10 -13 MHz). Credits: Mohan et al. (2019b,a)

solar and stellar activity studies that rely primarily on total-flux dynamic spectra without snapshot spectroscopic imaging are susceptible to contamination from co-temporal bright events, as discussed in Sect. 1.3. For the Sun, we can combine the coronal plasma diagnostics based on EUV to X-ray imaging, magnetic field diagnostics based on vector magnetograms (Bobra et al., 2014), and non-thermal radio emission variability in a spatially resolved manner along the axes of intensity and polarization to reliably constrain the emission mechanism and study correlations between the radio source variability and local dynamics at the associated active regions.

Figure 5 illustrates the use of spatially resolved dynamic spectra (SPREDS; Mohan and Oberoi, 2017), often also referred to as vector dynamic spectra (Chen et al., 2018), in separating the emission contributions from various co-temporal radio sources to the Sun-as-a-star dynamic spectrum. The figure shows MWA radio contours of the Sun during Nov 3, 2014, revealing two bright radio sources (A1 and A2). The zoomed-in images of the source regions at 94Å from the Atmospheric Imaging Assembly (AIA; Boerner et al., 2012) onboard Solar Dynamic Observatory (SDO; Pesnell et al., 2012) reveal their association with two different active regions. SPREDS for each radio source was made by recording the integrated flux density within an elliptical contour centered at the source for all spectroscopic snapshot images made with 0.5 s and 160 kHz averaging. The A1 source showed signatures of quasi-periodic intermittent groups of type III bursts in its SPREDS, co-temporal with a coronal jet event. Meanwhile, the active region associated with the A2 source underwent a microflare. The A2 source was active even in the pre-flare phase with QPPs in the radio emission at ∼s and ∼10-15 MHz scales. The coherent flux density of A2 and the strength of QPPs increased during the flare. It is evident that the burst features in the Sun-as-a-star dynamic spectrum arise as a superposition of emissions from A1 and A2. The SPREDS for each source showed very different quasi-periodic spectro-temporal variability, which were analysed in detail along with multiwaveband data and magnetic field modeling in multiple publications (Mohan et al., 2019b,a; Mohan, 2021b). These works could link the radio emission variability scales to physical scales at the active regions. Studies of this kind, spanning several events occurring in regions with varying physical parameters, will help characterize radio emission variability in flux density and polarization associated with different event types, and enable the development of robust physical diagnostics of the corresponding active regions.

The angular resolution, superior sensitivity, and high fidelity imaging of SKA will enable a robust characterisation of true source morphology and its spectro-temporal flux and polarisation variability for even weak radio transients. These studies will inform the sensitivity and spectro-temporal resolution required to track various types of activity in Sun-like stars. Applying solar-based insights and diagnostics to stellar dynamic spectra from the SKA telescopes could help infer the activity types and derive physical parameters of the unresolved active regions.

3.2 Generality of the standard flare model

Despite its general success, several solar and stellar flare observations tend to question the applicability of the standard flare model. Given the diverse physical conditions that can exist at or around active regions, it is possible that certain events could deviate, at least partially, from the standard model pathway (e.g. Veronig et al., 2002b; Tristan et al., 2023). Certain major observations that suggest the prevalence of non-standard processes beyond the standard flare model framework are the missing radio burst problem and the departures from the Neupert effect.

3.2.1 The missing radio bursts problem

As mentioned in Sect. 1.2, coherent radio bursts that outshine the disk-integrated solar/stellar flux density are produced by accelerated electron beams, and are key diagnostics of flare-associated reconnection, CMEs, and EPEs. Nevertheless, recent results from both stellar and solar observations appear to challenge this view.

Stellar case. Young M dwarfs ($\lesssim$1 Gyr) possess strong, dynamic magnetic fields and are among the most magnetically active stars in the Galaxy (Stepien, 1994b; Barnes, 2003; Donati and Landstreet, 2009; Vidotto et al., 2014). They produce frequent large flares and superflares ($E > 10^{33}$ erg) at rates of once every few days (Dal, 2020; Feinstein et al., 2020). Such flares are often associated with CMEs in the Sun, and are accompanied by coherent type II–IV bursts (McLean and Labrum, 1985; Gopalswamy, 2011; Miteva et al., 2017). Extensive searches have been carried out spanning hours to days on several active stars (e.g. Osten and Bastian, 2006; Osten et al., 2008; Villadsen and Hallinan, 2019) to detect solar-like burst types. Until now, a type IV has been detected in Proxima Cen (M5.5V; Zic et al., 2020), a type IV and long-duration type III in AD Leo (M4V; Mohan et al., 2024d), and a type II in StKM 1-1262 (M0V; Callingham et al., 2025). While the dearth of type II bursts in M dwarfs could be attributed to high Alfvén speeds suppressing coronal shocks (Alvarado-Gómez et al., 2022), the general lack of type III/IV or any flare-linked radio bursts in several strong stellar flares remains difficult to reconcile with the standard flare model (e.g. Smith et al., 2005; MacGregor et al., 2018).

Solar case. For the Sun, direct imaging and in-situ measurements of CMEs and SEPs allow detailed correlation studies between radio bursts and space-weather phenomena. Despite the high association rates, well above 85 - 90%, for type IV and II bursts with strong CMEs, only fewer than 5% of CMEs produce such bursts (Kumari et al., 2021b, 2023; Mohan et al., 2024a). Certain studies on type IV burst detectibility in metric wavebands have suggested the role of radiation absorption by dense structures in the non-detection of type IV emissions (e.g. Hillaris et al., 2016; Talebpour Sheshvan and Pohjolainen, 2018). Mohan et al. (2024a) compiled a catalog of type IV bursts in the 1 - 10 MHz band using decades of data from Wind and STEREO spacecraft that observed the same flare/CME event from multiple vantage points simultaneously. The authors showed that type IV emission exhibits a strong inherent beaming effect. Hence, the spacecraft that observed the burst source within ±60° line-of-sight always recorded the most intense event with relatively greater spectro-temporal extent. Mohan et al. (2024b) further noted that the favorable line-of-sight orientation of AD Leo's active latitudes may have aided in detecting its type IV burst. However, neither the occultation/absorption nor the inherent beaming effect can fully explain the non-detection of type II/IV bursts in previous AD Leo monitoring studies (Osten and Bastian, 2006; Villadsen and Hallinan, 2019), and in many solar flares/CMEs.

Another noteworthy finding in this context is that nearly 17% of HXR solar flares in a sample of 201 events studied by Benz et al. (2005) had no type of associated coherent radio bursts in the 100 - 4000 MHz band (Benz et al., 2007), even though HXR emission is another diagnostic of non-thermal electrons. All 201 events studied were of SXR flare class greater than C5, which are relatively strong events capable of driving CMEs (Yashiro et al., 2006; Kazachenko, 2023).

3.2.2 Departures from Neupert effect

In the standard flare model, magnetic reconnection not only drives electron beams upward into the corona, producing coherent bursts, but also downward producing impulsive microwave bursts observable with the SKA-Mid and HXR flares as they impact the chromosphere (see, Fig. 1b). Later, these energetic electrons dissipate energy heating the coronal loops, causing SXR flares. The Neupert effect, which relates the time integral of impulsive-phase emission to the thermal flare light

curve, is therefore a cornerstone of the standard flare model (see Sect. 1 Neupert, 1968). Besides, the GBR relationship that applies universally across flares in main-sequence stars highlights a tight correlation between SXR and microwave (5-8 GHz) flare peak flux densities. Despite this universal relationship between SXR and microwave flares, several multiwaveband stellar flare observations found cases where either SXR flares lacked radio counterparts or vice versa (Osten et al., 2005; Smith et al., 2005). Stellar flare studies that used U-band data to track impulsive chromospheric emissions also found cases where the Neupert effect seems to be violated (Osten et al., 2005; Tristan et al., 2023). Even in the Sun, statistical studies show that about 20 - 30% of the flares depart from the expected Neupert effect (e.g. Dennis and Zarro, 1993; Veronig et al., 2002a). For instance, Benz et al. (2017) reported a solar SXR flare which had no counterparts in HXR and 17 GHz. In another study, Struminsky and Zimovets (2008) reported microwave bursts that lasted well into the SXR flare decay phase with high flux density, indicating possible multiple episodes of particle acceleration. Thus, cases of continued particle acceleration without significant heating and thermal flares without clear impulsive phase emissions have been reported in many solar flares.

The SKA telescopes will be pivotal in tackling the problems of missing radio bursts and the deviations from the Neupert effect in the Sun and stars. High-dynamic range snapshot spectroscopic imaging of solar active regions enabled by the SKA telescopes will help detect and model even weak radio transients during X-ray/EUV flares in great detail. Additionally, these telescopes will enable sensitive long-duration multiwaveband monitoring studies of several cool stars, letting us identify and model the radio emission variability during optical/X-ray flares. These studies will help explore the general applicability of the standard flare model, characterise the solar and stellar events that deviate from the model, and compare their possible mechanisms.

3.3 Plasma emission and low frequency stellar radio bursts

With its spatial resolution and sensitivity, the SKA-Low telescope will be a superior instrument for the study of small-scale features on the Sun. Though radio wave scattering in the corona is expected to limit the instrument's spatial resolution to an extent, the SKA-Low telescope will still advance the range of observable spatial and temporal scales of variability in the solar corona, probing the time and spatial scales of energy release and particle acceleration. As noted earlier, there has been some success in obtaining dynamic spectra of radio bursts for nearby flare stars, but the observations are sporadic and do not provide a complete picture. There are reasons to think that plasma emission will have different properties in other types of stars. For example, free-free absorption decreases as the ambient temperature increases, so we expect that plasma emission will be detectable to higher frequencies than on the Sun, in stars with hotter coronae (e.g. White and Franciosini, 1995). However, coronae in some young active stars may be more extended and possess higher density than the Sun. In such a case, if electron beams are released low in the corona, they might not be able to propagate as far as they can on the Sun, leading to differences in the observed spectro-temporal variability in the radio dynamic spectrum compared to a solar flare of similar strength. Enhanced density in strong post-flare magnetic structures could also lead to significantly weak coherent emission flux density and impact the polarization signatures. SKA's sensitivity will allow a deeper and more thorough census of the occurrence of radio bursts on a wider sample of stellar types and ages than we can expect with current instrumentation. This

will allow us to better understand the nature of the coherent plasma emission process under varied physical scenarios existing in different stars, and contrast with the results from detailed solar imaging observations of various types of active phenomena.

3.4 Linear polarization

Recent confirmation of linear polarization in stellar (e.g. Zic et al., 2020; Bastian et al., 2022) and solar (Dey et al., 2025) radio emission is a potentially important development that can be exploited to investigate atmospheric structure. Conventional wisdom has always been that Faraday rotation in the solar or stellar atmosphere is so large at microwave frequencies that it will wipe out linear polarization even over narrow bandwidths, leaving just the circular polarization that is commonly observed and well understood in the solar context. Understanding how linear polarization can survive despite the known presence of a magnetized plasma atmosphere on active stars will likely reveal important information about stellar atmospheric structure. At present, we only have a very limited picture of the occurrence of linear polarization: we need to know much more about what types of stellar radio emission (burst, flare, quiescent) and what types of stars do and do not exhibit linear polarization to understand the role of coronal structure. The polarization sensitivity of the SKA telescopes will be pivotal for this field of study. Sensitive solar spectropolarimetry across the wide radio band will allow us to explore linear polarisation in various solar conditions and gain a better understanding of the underlying mechanism across different physical conditions existing in the Sun and stars.

3.5 Evolution of stellar flaring activity

Another paradigm in the solar-stellar field is that stars are born rapidly rotating and slow down as they age. Magnetic activity declines in older stars, since it is tied to P_{rot}. Observing the occurrence of stellar flares powered by magnetic activity is important, both for understanding the evolution of the star and because of the interest in the harshness of the space weather conditions close-in Earth-like exoplanets have to endure over the lifetime of different cool stellar types. Addressing the latter question is crucial for identifying stellar populations within the P_{rot}–age–T_{eff} parameter space that host relatively less hazardous environments for habitable-zone exoplanets and are therefore more likely to support biospheres. The sensitivity of the SKA telescopes will allow us to measure the activity levels of less active stars than we currently have access to, providing a much broader census of the evolution of stellar activity with stellar type and age.

3.6 Quiescent coronal activity diagnostics

Non-flaring or quiescent radio emission offers a powerful diagnostic of persistent non-thermal activity in stellar coronae (e.g. Bastian, 1990; Güdel, 2002; Villadsen and Hallinan, 2019). Quiescent microwave emission, within 1 - 30 GHz, is commonly detected from active stars, but its physical origin remains unclear. In principle, it could arise as thermal gyroresonance emission from a very hot corona with strong large scale magnetic field coverage (e.g. White et al., 1994). The associated spectral flux density is expected to increase with frequency. However, the observed quiescent microwave spectra of flare stars are typically flat (e.g. Guedel and Benz, 1989; Plant et al., 2024), suggesting the prevalence of long-lived non-thermal coronal emission.

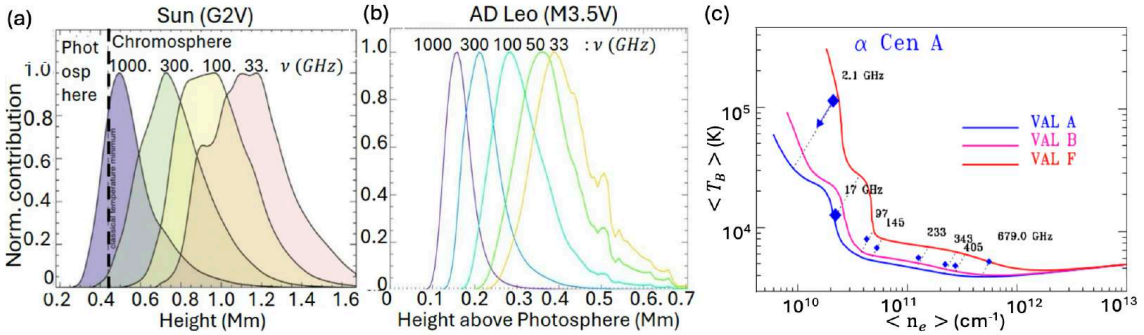

Figure 6: Formation of mm emission. *(a - b):* Normalised contribution function for various mm frequencies computed using 3D atmopsheric models for Sun and AD Leo. *(c):* Scaled solar chromopsheric model fit to the observed mm-$T_B(\nu)$ of α Cen A (Trigilio et al., 2018).

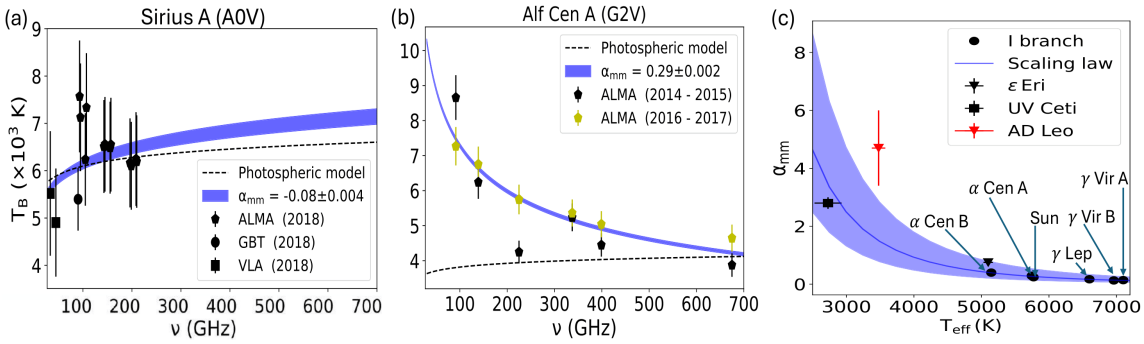

Figure 7: Quiescent mm-$T_B(\nu)$ of main-sequence stars. *(a - b):* The mm-$T_B(\nu)$, power-law spectral fit, and the photospheric model spectrum are for Sirius A and α Cen A. *(c):* Scaling law between α_{mm} and T_{eff} for 'I' branch cool stars, including Sun (Mohan et al., 2021, 2022, 2025). AD Leo, 'C' branch star (P_{rot}= 2.23 d, age~0.25 Gyr, T_{eff}~ 3500 K) deviates from the trend.

Studies on quiescent stellar emission at frequencies >15 GHz, using ALMA and JVLA, have yielded key insights into the steady heating of stellar chromospheres and transition regions (e.g. Osten et al., 2006; Bastian et al., 2018; Trigilio et al., 2018; White et al., 2020; Suresh et al., 2020; Mohan et al., 2021, 2022; Plant et al., 2024; Mohan et al., 2025). For instance, several studies have demonstrated thermal origin of the quiescent millimeter (mm) emission from stellar chromospheres, with longer wavelengths probing higher heights (e.g. Selhorst et al., 2014; Wedemeyer et al., 2016; White, 2004; Trigilio et al., 2018). The mm brightness temperature (mm-$T_B(\nu)$) spectrum thus acts as a linear thermometer probing the effective electron temperature across stellar chromospheric heights. Figure 6a shows the normalised contribution functions for various mm frequencies derived using a 3D solar atmospheric model, highlighting the varying emission formation height ranges as a function of frequency. Panel b in the figure estimates the same for AD Leo, using a 3D atmospheric model for the star (Wedemeyer et al., 2013). Figure 6c shows the results of a data-constrained modeling of the observed mm-$T_B(\nu)$ of αCen A. The $T_B(\nu)$ values at various frequencies, including portions of the SKA-Mid's operational band, are consistent with the range predicted by scaled solar chromospheric thermal emission models (VAL A, B, and F).

In a sample of ALMA-detected stars, Mohan et al. (2021) showed that mm-$T_B(\nu)$ of F-M type stars with an active outer atmosphere deviated significantly from a purely photospheric model spectrum

computed using the PHOENIX code given the stellar parameters (Hauschildt and Baron, 1999). Meanwhile, the A-type stars in the sample that lack active chromospheres agreed with the respective photospheric emission model. Figure 7 shows the mm-$T_B(\nu)$ data points, the best-fit power-law model, and the PHOENIX-based photospheric model for an A and a G dwarf. In fact, the mm-$T_B(\nu)$ spectral index, α_{mm} ($T_B(\nu) \sim \nu^{-\alpha_{mm}}$), which is related to the strength of chromospheric heating, scales with T_{eff} (Mohan et al., 2021, 2025). Figure 7d shows the scaling law between α_{mm} and T_{eff}, for a sample of stars belonging to the 'I' branch activity population, like our Sun. Clearly AD Leo, which is a fast-rotating 'C' branch star, deviates from the trend.

With the combined capabilities of SKA, ALMA, and JVLA, it will be possible to model the quiescent sub-THz spectrum for stars across the P_{rot}–age–T_{eff} plane and to derive physically meaningful metrics of quasi-steady heating and activity across the corona to chromosphere, and explore its correlations with stellar magnetic field and plasma parameters. SKA will be crucial in providing diagnostics in the 5 - 15 GHz range.

3.7 Evolution of the Sun and solar analogs in time

Understanding how the activity of our Sun evolved over ages and will evolve into its future is fundamental to not only solar long-term activity research but also the question of the exposure of habitable zone planets (Venus, Earth, and Mars) to the evolving space weather in the past and into the next few gigayears. The study of magnetic activity in solar-like stars at different evolutionary stages has advanced significantly due to large surveys by various space ground-based high energy spectropolarimetric facilities (e.g. Marsden et al., 2014; van Saders et al., 2016; Davenport et al., 2019; Feinstein et al., 2020). The sensitive radio observations from SKA can provide valuable constraints on magnetic field and wind properties (e.g. González and Cantó, 2002). Extending SPREDS-based active region and space weather diagnostics on long-term stellar flare datasets will help infer the occurrence rates and properties of active events, especially those with potential space weather consequences. Performing such studies on long-term monitoring datasets from Sun-like stars of varying ages will be crucial in obtaining a statistical picture of activity evolution in a typical solar-like star during its lifetime (Güdel, 2020).

4 Conclusions

The various kinds of magnetic activity in the cool main-sequence stars are often observed as enhanced emissions or flares in the radio to X-ray bands. The Sun, with its unique spatially resolved observations and in-situ energetic particle measurements, provides a detailed view of how active regions evolve and produce flares, which cause major space weather impacts. The wealth of multiwavelength solar imaging datasets serves as the benchmark for constructing disk-integrated Sun-as-a-star diagnostics of active regions and space weather, extendable to stellar flare observations. Of the various flare signatures, radio bursts provide key diagnostics of magnetic reconnection and particle acceleration, which are the central ingredients of the standard flare model.

The field of solar–stellar activity seeks to apply solar-based models and Sun-as-a-star diagnostics to interpret unresolved stellar active regions and to assess space-weather conditions during both active and quasi-steady emission phases. Comparative analyses of solar and stellar events also allow us to

identify departures from the standard flare and activity framework, study the long-term evolution of magnetic activity in Sun-like stars, and investigate both quiescent and active atmospheric conditions across different stellar types. Since this young and rapidly evolving field depends on both solar and stellar observations, the advances enabled by the SKA telescopes in both domains will be highly beneficial to solar–stellar activity research. The frequencies probed by the SKA telescopes, 0.05 - 15 GHz will probe a variety of non-thermal particle acceleration processes in the Sun and stars across heights from low corona to interplanetary space. The high cadence, high dynamic range, spectro-polarimetric imaging of the Sun, enabled by the SKA telescopes, will allow the exploration of robust Sun-as-a-star diagnostics of active regions and space weather. On the stellar side, the exceptional sensitivity and survey speed of the SKA telescopes will enable high-cadence, spectro-polarimetric observations of stellar flare dynamic spectra from several stars within several tens to a few hundred parsecs. These stellar datasets and the Sun-as-a-star diagnostics based on detailed solar imaging studies will facilitate various comparative solar stellar science cases. Some of these science cases are discussed in the chapter, namely, the test of the standard flare model across stellar systems, exploring radio emission mechanisms under varying stellar and solar atmospheric conditions, modeling quiescent atmospheric activity in the sun and stars, and exploring the evolution of activity and space weather conditions in stars across P_{rot}-age-T_{eff} parameter space.

Acknowledgements AM is partly supported by NASA's STEREO project and the LWS program. SW acknowledges support by the Research Council of Norway, project number 325491, through its Centres of Excellence scheme, project number 262622 (RoCS). AM acknowledges the helpful discussions with Dr. Tim Bastian.

References

S. Akiyama, N. Gopalswamy, S. Yashiro, and P. Mäkelä. *Pub. Astron. Soc. Japan*, 65:S15, Dec. 2013. doi: 10.1093/pasj/65.sp1.S15.

C. Alissandrakis, A. Hillaris, C. Bouratzis, and S. Armatas. *Universe*, 9(10):442, Sept. 2023. doi: 10.3390/universe9100442.

C. E. Alissandrakis and D. E. Gary. *Frontiers in Astronomy and Space Sciences*, 7:77, Jan. 2021. doi: 10.3389/fspas.2020.591075.

J. D. Alvarado-Gómez et al. *Astronomische Nachrichten*, 343(4):e10100, May 2022. doi: 10.1002/asna.20210100.

K. Arzner and A. Magun. *Astron. Astrophys.*, 351:1165–1189, Nov. 1999.

M. J. Aschwanden. *Solar Phys.*, 111:113–136, Mar. 1987. doi: 10.1007/BF00145445.

M. J. Aschwanden, Y. Xu, and J. Jing. *Astrophys. J.*, 797(1):50, Dec. 2014. doi: 10.1088/0004-637X/797/1/50.

M. J. Aschwanden et al. *Astrophys. J.*, 802(1):53, Mar. 2015. doi: 10.1088/0004-637X/802/1/53.

S. A. Barnes. *Astrophys. J.*, 586(1):464–479, mar 2003. doi: 10.1086/367639. URL https://doi.org/10.1086/367639.

D. Bashi et al. *Astron. Astrophys.*, 643:A106, Nov. 2020. doi: 10.1051/0004-6361/202038881.

T. S. Bastian. *Solar Phys.*, 130(1-2):265–294, Dec. 1990. doi: 10.1007/BF00156794.

T. S. Bastian et al. *Astrophys. J.*, 857(2):133, Apr. 2018. doi: 10.3847/1538-4357/aab3cb.

T. S. Bastian, W. D. Cotton, and G. Hallinan. *Astrophys. J.*, 935(2):99, Aug. 2022. doi: 10.3847/1538-4357/ac7d57.

A. O. Benz and M. Guedel. *Astron. Astrophys.*, 285:621–630, May 1994.

A. O. Benz, P. C. Grigis, A. Csillaghy, and P. Saint-Hilaire. *Solar Phys.*, 226(1):121–142, Jan. 2005. doi: 10.1007/s11207-005-5254-5.

A. O. Benz, R. Brajša, and J. Magdalenić. *Solar Phys.*, 240(2):263–270, Feb. 2007. doi: 10.1007/s11207-007-0365-9.

A. O. Benz, M. Battaglia, and M. Güdel. *Solar Phys.*, 292(10):151, Oct. 2017. doi: 10.1007/s11207-017-1175-3.

M. G. Bobra et al. *Solar Phys.*, 289:3549–3578, Sept. 2014. doi: 10.1007/s11207-014-0529-3.

P. Boerner et al. *Solar Phys.*, 275(1-2):41–66, Jan. 2012. doi: 10.1007/s11207-011-9804-8.

T. M. Brown. *Astrophys. J.*, 789(2):101, July 2014. doi: 10.1088/0004-637X/789/2/101.

J. R. Callingham et al. *Nature*, 647(8090):603–607, Nov. 2025. doi: 10.1038/s41586-025-09715-3.

H. V. Cane, W. C. Erickson, and N. P. Prestage. *Journal of Geophysical Research (Space Physics)*, 107(A10):1315, Oct. 2002. doi: 10.1029/2001JA000320.

E. P. Carley et al. *Nature Communications*, 10:2276, May 2019. doi: 10.1038/s41467-019-10204-1.

B. Chen et al. *Astrophys. J.*, 866(1):62, Oct. 2018. doi: 10.3847/1538-4357/aadb89.

H. A. Dal. *Mon. Not. Roy. Astron. Soc.*, 495(4):4529–4541, July 2020. doi: 10.1093/mnras/staa1484.

J. R. A. Davenport et al. *Astrophys. J.*, 871(2):241, Feb. 2019. doi: 10.3847/1538-4357/aafb76.

B. R. Dennis. *Solar Phys.*, 100:465, Oct. 1985. doi: 10.1007/BF00158441.

B. R. Dennis and D. M. Zarro. *Solar Phys.*, 146(1):177–190, July 1993. doi: 10.1007/BF00662178.

S. Dey, D. Kansabanik, D. Oberoi, and S. Mondal. *Astrophys. J. Lett.*, 988(2):L73, 2025. doi: 10.3847/2041-8213/adef0e.

J. F. Donati and J. D. Landstreet. *Annu. Rev. Astron. Astrophys.*, 47(1):333–370, Sept. 2009. doi: 10.1146/annurev-astro-082708-101833.

G. A. Dulk. *Annu. Rev. Astron. Astrophys.*, 23:169–224, Jan. 1985. doi: 10.1146/annurev.aa.23.090185.001125.

A. Endo et al. *Pub. Astron. Soc. Japan*, 62:1341–1349, Oct. 2010. doi: 10.1093/pasj/62.5.1341.

A. D. Feinstein et al. *Astronom. J.*, 160(5):219, Nov. 2020. doi: 10.3847/1538-3881/abac0a.

D. E. Gary and G. J. Hurford. In D. E. Gary and C. U. Keller, editors, *Astrophysics and Space Science Library*, volume 314 of *Astrophysics and Space Science Library*, page 71, Sept. 2004. doi: 10.1007/1-4020-2814-8_4.

D. E. Gary, H. Wang, N. Nitta, and T. Kosugi. *Astrophys. J.*, 464:965, June 1996. doi: 10.1086/177384.

D. E. Gary et al. *Astrophys. J.*, 863(1):83, aug 2018. doi: 10.3847/1538-4357/aad0ef. URL https://doi.org/10.3847/1538-4357/aad0ef.

G. A. Gary. *Solar Phys.*, 203:71–86, Oct. 2001. doi: 10.1023/A:1012722021820.

R. F. González and J. Cantó. *The Astrophysical Journal*, 580(1):459, nov 2002. doi: 10.1086/343037. URL https://doi.org/10.1086/343037.

N. Gopalswamy. *Geophysical Monograph Series*, 119:123, Jan. 2000. doi: 10.1029/GM119p0123.

N. Gopalswamy. *Geophys. Res. Lett.*, 30(12):8013, June 2003. doi: 10.1029/2003GL017277.

N. Gopalswamy. In H. O. Rucker, W. S. Kurth, P. Louarn, and G. Fischer, editors, *Planetary, Solar and Heliospheric Radio Emissions (PRE VII)*, pages 325–342, Jan. 2011.

N. Gopalswamy, K. Shibasaki, and M. Salem. *JoAA*, 21(3-4):413–417, Sept. 2000. doi: 10.1007/BF02702435.

N. Gopalswamy et al. *Journal of Geophysical Research (Space Physics)*, 110(A12):A12S07, Dec. 2005. doi: 10.1029/2005JA011158.

N. Gopalswamy et al. *Astrophys. J. Lett.*, 868(2):L19, Dec. 2018. doi: 10.3847/2041-8213/aaef36.

M. Güdel. *Annu. Rev. Astron. Astrophys.*, 40:217–261, Jan. 2002. doi: 10.1146/annurev.astro.40.060401.093806.

M. Güdel. *Space Sci. Rev.*, 216(8):143, Dec. 2020. doi: 10.1007/s11214-020-00773-9.

M. Gudel, J. H. M. M. Schmitt, et al. *Astrophys. J.*, 415:236, Sept. 1993. doi: 10.1086/173158.

M. Guedel and A. O. Benz. *Astron. Astrophys.*, 211:L5–L8, Feb. 1989.

M. Guedel, A. O. Benz, et al. *Astrophys. J.*, 471:1002, Nov. 1996. doi: 10.1086/178027.

M. Guedel et al. *Astron. Astrophys.*, 302:775, Oct. 1995.

Y. Gupta et al. *Current Science*, 113(4):707–714, Aug. 2017. doi: 10.18520/cs/v113/i04/707-714.

R. A. Harrison, P. Bryans, G. M. Simnett, and M. Lyons. *Astron. Astrophys.*, 400:1071–1083, Mar. 2003. doi: 10.1051/0004-6361:20030088.

P. H. Hauschildt and E. Baron. *J. Comput. Appl. Math.*, 109(1):41–63, Sept. 1999.

A. Hillaris, C. Bouratzis, and A. Nindos. *Solar Phys.*, 291(7):2049–2069, Aug. 2016. doi: 10.1007/s11207-016-0946-6.

T. Hirayama. *Solar Phys.*, 34(2):323–338, Feb. 1974. doi: 10.1007/BF00153671.

H. S. Hudson, L. W. Acton, et al. *Astrophys. J.*, 470:629, Oct. 1996. doi: 10.1086/177894.

K. Iwai et al. In T. Sekii, T. Watanabe, and T. Sakurai, editors, *Hinode-3: The 3rd Hinode Science Meeting*, volume 454 of *Astronomical Society of the Pacific Conference Series*, page 249, Aug 2012.

K. Iwai et al. *Astrophys. J.*, 789:4, July 2014. doi: 10.1088/0004-637X/789/1/4.

N. L. S. Jeffrey, L. Fletcher, and N. Labrosse. *Astrophys. J.*, 836(1):35, Feb. 2017. doi: 10.3847/1538-4357/836/1/35.

J. Jonas and MeerKAT Team. In *MeerKAT Science: On the Pathway to the SKA*, page 1, Jan. 2016. doi: 10.22323/1.277.0001.

M. D. Kazachenko. *Astrophys. J.*, 958(2):104, Dec. 2023. doi: 10.3847/1538-4357/ad004e.

E. P. Kontar et al. *Phys. Rev. Let.*, 118(15):155101, Apr. 2017a. doi: 10.1103/PhysRevLett.118.155101.

E. P. Kontar et al. *Nature Communications*, 8:1515, Nov. 2017b. doi: 10.1038/s41467-017-01307-8.

A. F. Kowalski. *LRSP*, 21(1):1, Apr. 2024. doi: 10.1007/s41116-024-00039-4.

A. Kumari, D. E. Morosan, and E. K. J. Kilpua. *Astrophys. J.*, 906(2):79, Jan. 2021a. doi: 10.3847/1538-4357/abc878.

A. Kumari, D. E. Morosan, and E. K. J. Kilpua. *Astrophys. J.*, 906(2):79, Jan. 2021b. doi: 10.3847/1538-4357/abc878.

A. Kumari, D. E. Morosan, E. K. J. Kilpua, and F. Daei. *Astron. Astrophys.*, 675:A102, July 2023. doi: 10.1051/0004-6361/202244015.

A. A. Kuznetsov, G. D. Fleishman, G. M. Nita, and S. A. Anfinogentov. *Astrophys. J.*, 991(2):186, Oct. 2025. doi: 10.3847/1538-4357/adfc4b.

J. Lee et al. *Astrophys. J.*, 585(1 I):524–535, Mar. 2003. ISSN 0004-637X. doi: 10.1086/346024.

C. Y. Li et al. *Solar Phys.*, 292:82, June 2017. doi: 10.1007/s11207-017-1108-1.

A. Lysenko et al. *Physics-Uspekhi*, 63, 06 2019. doi: 10.3367/UFNe.2019.06.038757.

M. A. MacGregor et al. *Astrophys. J. Lett.*, 855(1):L2, Mar. 2018. doi: 10.3847/2041-8213/aaad6b.

S. C. Marsden et al. *Mon. Not. Roy. Astron. Soc.*, 444(4):3517–3536, Nov. 2014. doi: 10.1093/mnras/stu1663.

L. Mashonkina, T. Sitnova, and A. K. Belyaev. *Astron. Astrophys.*, 605:A53, Sept. 2017. doi: 10.1051/0004-6361/201731236.

P. I. McCauley et al. *Astrophys. J.*, 851(2):151, Dec. 2017. doi: 10.3847/1538-4357/aa9cee.

D. McLean and N. Labrum. *Solar Radio Astrophysics*. Cambridge University Press, 1985.

R. Miteva, S. W. Samwel, et al. *JSWSC*, 7:A37, Dec. 2017. doi: 10.1051/swsc/2017035.

A. Mohan. *Astron. Astrophys.*, 655:A77, Nov. 2021a. doi: 10.1051/0004-6361/202142029.

A. Mohan. *Astrophys. J. Lett.*, 909(1):L1, Mar. 2021b. doi: 10.3847/2041-8213/abe70a.

A. Mohan and D. Oberoi. *Solar Phys.*, 292:168, Nov. 2017. doi: 10.1007/s11207-017-1193-1.

A. Mohan, P. I. McCauley, D. Oberoi, and A. Mastrano. *Astrophys. J.*, 883(1):45, Sept. 2019a. doi: 10.3847/1538-4357/ab3a94.

A. Mohan, S. Mondal, D. Oberoi, and C. J. Lonsdale. *Astrophys. J.*, 875(2):98, Apr. 2019b. doi: 10.3847/1538-4357/ab0ae5.

A. Mohan et al. *Astron. Astrophys.*, 655:A113, Nov. 2021. doi: 10.1051/0004-6361/202142095.

A. Mohan et al. *Astron. Astrophys.*, 664:L9, Aug. 2022. doi: 10.1051/0004-6361/202244385.

A. Mohan et al. *Astrophys. J.*, 971(1):86, Aug. 2024a. doi: 10.3847/1538-4357/ad5315.

A. Mohan et al. *arXiv e-prints*, art. arXiv:2410.00787, Oct. 2024b. doi: 10.48550/arXiv.2410.00787.

A. Mohan, N. Gopalswamy, H. Raju, and S. Akiyama. *Astron. Astrophys.*, 691:L8, Nov. 2024c. doi: 10.1051/0004-6361/202451072.

A. Mohan, S. Mondal, S. Wedemeyer, and N. Gopalswamy. *Astron. Astrophys.*, 686:A51, June 2024d. doi: 10.1051/0004-6361/202347924.

A. Mohan et al. *Astrophys. J.*, 989(1):20, Aug. 2025. doi: 10.3847/1538-4357/ade9bf.

S. Mondal and D. Oberoi. *Astrophys. J.*, 920(1):11, Oct. 2021. doi: 10.3847/1538-4357/ac1076.

D. E. Morosan, P. Zucca, D. S. Bloomfield, and P. T. Gallagher. *Astron. Astrophys.*, 589:L8, May 2016. doi: 10.1051/0004-6361/201628392.

D. E. Morosan, E. K. J. Kilpua, E. P. Carley, and C. Monstein. *Astron. Astrophys.*, 623:A63, Mar. 2019. doi: 10.1051/0004-6361/201834510.

V. M. Nakariakov and V. F. Melnikov. *Space Sci. Rev.*, 149(1-4):119–151, Dec. 2009. doi: 10.1007/s11214-009-9536-3.

K. Namekata et al. *Astrophys. J.*, 961(1):23, Jan. 2024. doi: 10.3847/1538-4357/ad0b7c.

W. M. Neupert. *Astrophys. J. Lett.*, 153:L59, July 1968. doi: 10.1086/180220.

A. Nindos et al. *Astrophys. J. Supp. Series*, 130(2):485–499, oct 2000. doi: 10.1086/317355. URL https://doi.org/10.1086/317355.

N. V. Nitta and T. Mulligan. *Solar Phys.*, 292(9):125, Sept. 2017. doi: 10.1007/s11207-017-1147-7.

R. W. Noyes et al. *Astrophys. J.*, 279:763–777, Apr. 1984. doi: 10.1086/161945.

D. Oberoi, R. Sharma, and A. E. E. Rogers. *Solar Phys.*, 292(6):75, June 2017. doi: 10.1007/s11207-017-1096-1.

R. A. Osten and T. S. Bastian. *Astrophys. J.*, 637(2):1016–1024, Feb. 2006. doi: 10.1086/498410.

R. A. Osten et al. *Astrophys. J.*, 621(1):398–416, Mar. 2005. doi: 10.1086/427275.

R. A. Osten et al. *Astrophys. J.*, 647(2):1349–1374, Aug. 2006. doi: 10.1086/504889.

R. A. Osten et al. *Astrophys. J.*, 674(2):1078–1085, Feb. 2008. doi: 10.1086/525013.

W. D. Pesnell, B. J. Thompson, and P. C. Chamberlin. *Solar Phys.*, 275(1-2):3–15, Jan. 2012. doi: 10.1007/s11207-011-9841-3.

A. A. Pevtsov, G. H. Fisher, et al. *Astrophys. J.*, 598(2):1387–1391, Dec. 2003. doi: 10.1086/378944.

K. Plant, G. Hallinan, and T. Bastian. *Astrophys. J.*, 970(1):56, July 2024. doi: 10.3847/1538-4357/ad4356.

H. A. S. Reid and H. Ratcliffe. *Research in Astronomy and Astrophysics*, 14:773–804, July 2014. doi: 10.1088/1674-4527/14/7/003.

P. Saint-Hilaire, N. Vilmer, and A. Kerdraon. *Astrophys. J.*, 762:60, Jan. 2013. doi: 10.1088/0004-637X/762/1/60.

K. Saito, M. Makita, K. Nishi, and S. Hata. *Annals of the Tokyo Astronomical Observatory*, 12(2):51–173, Jan. 1970.

C. L. Selhorst et al. *The Astrophysical Journal*, 790(2):134, jul 2014. doi: 10.1088/0004-637x/790/2/134. URL https://doi.org/10.1088/0004-637x/790/2/134.

I. N. Sharykin, E. P. Kontar, and A. A. Kuznetsov. *Solar Phys.*, 293:115, Aug. 2018. doi: 10.1007/s11207-018-1333-2.

K. Shibasaki, C. E. Alissandrakis, and S. Pohjolainen. *Solar Phys.*, 273(2):309–337, Nov. 2011. doi: 10.1007/s11207-011-9788-4.

K. Shibata, S. Masuda, et al. *Astrophys. J. Lett.*, 451:L83, Oct. 1995. doi: 10.1086/309688.

M. Shimojo et al. *The Astrophysical Journal*, 848(1):62, oct 2017. doi: 10.3847/1538-4357/aa8c75. URL https://doi.org/10.3847/1538-4357/aa8c75.

K. Smith, M. Güdel, and M. Audard. *Astron. Astrophys.*, 436(1):241–251, June 2005. doi: 10.1051/0004-6361:20042054.

K. Stepien. *Astron. Astrophys.*, 292:191–207, Dec. 1994a.

K. Stepien. *Astron. Astrophys.*, 292:191–207, Dec. 1994b.

A. B. Struminsky and I. V. Zimovets. *Astronomy Letters*, 34(10):704–712, Oct. 2008. doi: 10.1134/S106377370810006X.

A. Suresh et al. *Astrophys. J.*, 904(2):138, Dec. 2020. doi: 10.3847/1538-4357/abc004.

N. Talebpour Sheshvan and S. Pohjolainen. *Solar Phys.*, 293(11):148, Nov. 2018. doi: 10.1007/s11207-018-1371-9.

A. S. H. To et al. *Astrophys. J.*, 948(2):121, May 2023. doi: 10.3847/1538-4357/acbc1b.

S. Toriumi et al. *ApJS*, 262(2):46, Oct. 2022. doi: 10.3847/1538-4365/ac8b15.

C. Trigilio et al. *Mon. Not. Roy. Astron. Soc.*, 481(1):217–225, Nov. 2018. doi: 10.1093/mnras/sty2280.

I. I. Tristan et al. *Astrophys. J.*, 951(1):33, July 2023. doi: 10.3847/1538-4357/acc94f.

M. P. van Haarlem et al. *Astron. Astrophys.*, 556:A2, Aug. 2013. doi: 10.1051/0004-6361/201220873.

J. L. van Saders et al. *Nature*, 529(7585):181–184, Jan. 2016. doi: 10.1038/nature16168.

J. E. Vernazza, E. H. Avrett, and R. Loeser. *Astrophys. J. Supp. Series*, 45:635–725, Apr. 1981. doi: 10.1086/190731.

A. Veronig et al. *Astron. Astrophys.*, 392:699–712, Sept. 2002a. doi: 10.1051/0004-6361:20020947.

A. Veronig et al. *Astron. Astrophys.*, 392:699–712, Sept. 2002b. doi: 10.1051/0004-6361:20020947.

A. M. Veronig et al. *NatAs*, 5:697–706, Jan. 2021. doi: 10.1038/s41550-021-01345-9.

A. A. Vidotto et al. *Mon. Not. Roy. Astron. Soc.*, 441(3):2361–2374, July 2014. doi: 10.1093/mnras/stu728.

J. Villadsen and G. Hallinan. *ApJ*, 871(2):214, Feb. 2019. doi: 10.3847/1538-4357/aaf88e.

S. Wedemeyer, H. G. Ludwig, and O. Steiner. *Astronomische Nachrichten*, 334(1-2):137–140, Feb. 2013. doi: 10.1002/asna.201211741.

S. Wedemeyer et al. *Space Sci. Rev.*, 200(1-4):1–73, Apr. 2016. doi: 10.1007/s11214-015-0229-9.

J. A. White et al. *Astrophys. J.*, 894(1):76, May 2020. doi: 10.3847/1538-4357/ab8467.

S. M. White. *New Astron. Rev.*, 48(11-12):1319–1326, Dec. 2004. doi: 10.1016/j.newar.2004.09.014.

S. M. White and E. Franciosini. *Astrophys. J.*, 444:342, May 1995. doi: 10.1086/175609.

S. M. White and M. R. Kundu. *Solar Phys.*, 174(1-2):31–52, Aug. 1997. doi: 10.1023/A:1004975528106.

S. M. White, P. D. Jackson, and M. R. Kundu. *Astrophys. J. Supp. Series*, 71:895, Dec. 1989. doi: 10.1086/191401.

S. M. White, J. Lim, and M. R. Kundu. *Astrophys. J.*, 422:293, Feb. 1994. doi: 10.1086/173727.

S. M. White, R. J. Thomas, J. W. Brosius, and M. R. Kundu. *Astrophys. J. Lett.*, 534(2):L203–L206, May 2000. doi: 10.1086/312673.

L. M. Winter and K. Ledbetter. *Astrophys. J.*, 809(1):105, Aug. 2015. doi: 10.1088/0004-637X/809/1/105.

S. Yashiro, S. Akiyama, et al. *Astrophys. J. Lett.*, 650(2):L143–L146, Oct. 2006. doi: 10.1086/508876.

L. Zhang, D. Wu, L. Chen, and Z. Ning. *Astrophys. J.*, 977(2):260, Dec. 2024. doi: 10.3847/1538-4357/ad95ea.

Y.-A. Zhou, J. Hong, Y. Li, and M. D. Ding. *Astrophys. J.*, 926(2):223, Feb. 2022. doi: 10.3847/1538-4357/ac497e.

A. Zic, T. Murphy, Lynch, et al. *Astrophys. J.*, 905(1):23, Dec. 2020. doi: 10.3847/1538-4357/abca90.